

TuNet: End-to-end Hierarchical Brain Tumor Segmentation using Cascaded Networks

Minh H. Vu¹, Tufve Nyholm¹, and Tommy Löfstedt¹

Department of Radiation Sciences, Umeå University, Umeå, Sweden
 minh.vu@umu.se

Abstract. Glioma is one of the most common types of brain tumors arising in the glial cells in the human brain and spinal cord. In addition to the threat of death, glioma treatment is also very costly. Hence, automatic and accurate segmentation and measurement from the early stages are critical in order to prolong the survival rates of the patients and to reduce the costs of health care. In the present work, we propose a novel end-to-end cascaded network for semantic segmentation that utilizes the hierarchical structure of the tumor sub-regions with ResNet-like blocks and Squeeze-and-Excitation modules after each convolution and concatenation block. By utilizing cross-validation, an average ensemble technique, and a simple post-processing technique, we obtained dice scores of 90.34, 81.12, and 78.42 and Hausdorff Distances (95th percentile) of 4.32, 6.28, and 3.70 for the whole tumor, tumor core, and enhancing tumor, respectively, on the online validation set.

1 Introduction

Glioma is among the most aggressive and dangerous types of cancer [11], leading, for instance, to around 80 % and 75 % of all malignant brain tumors diagnosed in the United States [8] and Sweden [1], respectively. Gliomas with different prognosis and numerous heterogeneous histological sub-regions, such as edema, necrotic core, and enhancing and non-enhancing tumor core, are classified into four world health organisation (WHO) grades according to their aggressiveness: low grade glioma (LGG) (class I and II, considered as slow-growing), and high grade glioma (HGG) (class III and IV, considered as fast-growing).

The aim of the Brain Tumors in Multimodal Magnetic Resonance Imaging Challenge 2019 (BraTS19) [16,4,5,3,2] is in evaluating and finding new state-of-the-art methods for tumor segmentation and to set a gold standard for the segmentation of intrinsically heterogeneous brain tumors. BraTS19 provided a large data set comprising multi-institutional pre-operative magnetic resonance imaging (MRI) scans with four sequences: post-contrast T1-weighted (T1c), T2-weighted (T2w), T1-weighted (T1w), and T2 Fluid Attenuated Inversion Recovery (FLAIR). Masks were annotated manually by one to four raters followed by improvements by expert raters. The segmentation performance of the participants was measured using Sørensen-Dice coefficient (DSC), sensitivity, specificity, and 95th percentile of the Hausdorff distance (HD95).

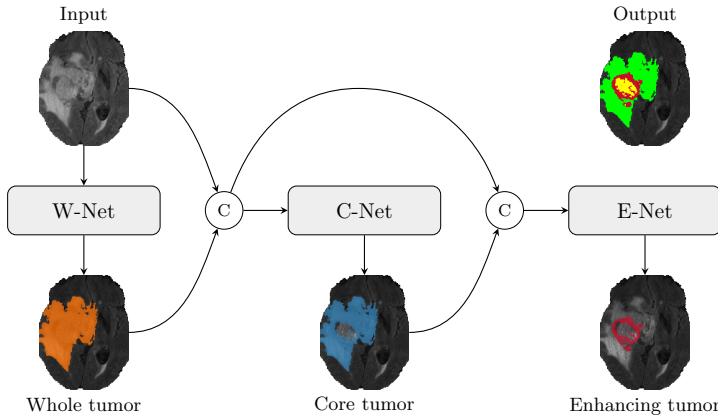


Fig. 1: Schematic visualization of TuNet. The input is the MRI volumes as four different channels, while the output is the predicted masks for the three labels: the necrotic and non-enhancing tumor core (NCR/NET—label 1, green), the peritumoral edema (ED—label 2, yellow) and the GD-enhancing tumor (ET—label 3, red). First, the multi-modal input is fed into the W-Net to generate a probability map of the whole tumor region (orange) including labels 1, 2 and 3. Second, the concatenation of the whole tumor probability map and the input is passed through the C-Net to produce the tumor core probability map (blue) including labels 1 and 3. Third, the two obtained maps from W-Net and C-Net are concatenated with the multi-modal input and then fed into the E-Net to generate an enhancing tumor probability map including label 3. Last, the outputs of W-Net, C-Net, and E-Net are merged to produce the final brain tumor mask.

Traditional discriminative approaches, such as Support-vector Machines [6], have been widely used in medical image segmentation. In recent years, Convolutional Neural Networks (CNNs) have achieved state-of-the-art performance in numerous computer vision tasks. In the field of medical image segmentation, a fully convolutional encoder-decoder neural network named U-Net, introduced by Ronneberger *et al.* [18], has received a lot of attention in recent years. With its success, it is unsurprising that the U-Net has motivated many top-ranking teams in segmentation competitions in previous years [13,7,17,19].

Kittrungrotsakul *et al.* [15] presented CasDetNet-CLSTM to detect mitotic events in 4D microscopic images by introducing a connection between a region-based convolutional neural network and convolutional long short-term memory. In the BraTS18, instead of proposing a new network, Isensee *et al.* [13] focused on the training process, and made only minor modifications to the U-Net, used additional training data, and applied a simple post-processing technique. Myronenko [17] was the winner of BraTS18 by introducing a U-Net-like network

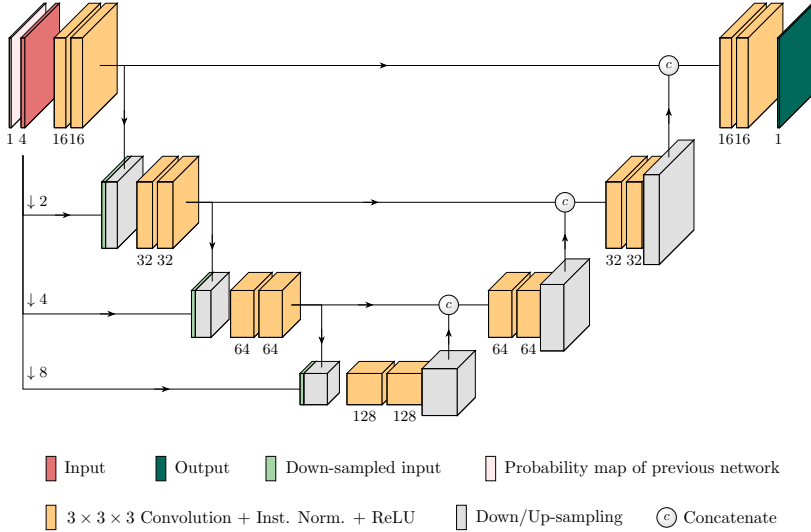


Fig. 2: Our C-Net and E-Net with a U-Net backbone. The W-Net does not include the probability map produced by a previous sub-network. To enrich the feature map at each level in the encoder part, we concatenate the down-sampled original input (light green) with the down-sampled output (grey) of the convolution block (yellow). Each convolution block comprises a convolution operation, an instance normalization followed by a ReLU activation function. The W-Net constrains the C-Net, while the C-Net constrains the E-Net. The E-Net functions as a regularizer for the C-Net, while the C-Net plays the same role for the W-Net.

with an asymmetrically large encoder and a Variational Auto-Encoder (VAE) branch to reconstruct the input image to add guidance and regularization to the encoder part of the network.

In another work, Wang *et al.* [19] proposed an encoder-decoder cascaded anisotropic CNN, that won the second place in the BraTS17, that hierarchically segments the whole tumor, tumor core, and enhancing tumor core sequentially by separating the complex brain tumor segmentation problem into three binary segmentation problems. We argue that: (1) the training process employed in [19] might be time-consuming as there are three separate binary segmentation problems, and (2) the lack of regularization could lead to overfitting.

Motivated by the successes of the cascaded anisotropic network, introduced in [19], and the VAE branch, presented in [17], we propose a novel architecture, denoted End-to-end Hierarchical Tumor Segmentation using Cascaded Networks (TuNet). TuNet exploits separating a complex problem into less challenging sub-problems, and also attempts to avoid overfitting by using heavy regularization through multi-task learning. In the present work, we constructed three U-Net-

like networks, each was used to segment a specific tumor region, *i.e.* whole tumor, core tumor, and enhancing tumor. We connected the three sub-networks to form an end-to-end cascaded network in the hope that three sub-networks could mutually regularize each other to prevent overfitting and reduce the training time.

2 Methods

Motivated by these drawbacks in [19], we thus propose a framework that we expect not only utilizes region-based optimization like that but also we hypothesise that it will prevent or reduce overfitting.

2.1 Cascaded Architecture

Figure 1 illustrates the proposed end-to-end cascaded architecture. As in [19], we employed three encoder-decoder networks to cope with the three aforementioned tumor regions. We denote them W-Net (whole tumor network), C-Net (core tumor network), and E-Net (enhancing tumor network). In our proposed approach, instead of using three separate networks, we joined them together to form an end-to-end cascaded network.

2.2 Segmentation Network

Figure 2 shows the proposed symmetric encoder-decoder C-Net and E-Net. The patch size was set to $80 \times 96 \times 64$. Note that the probability map (pink) was concatenated with the input image as a first step for the C-Net and the E-Net, but not for the W-Net. We also concatenated the max-pooled feature maps with the down-sampled input (light green) in order to enhance the feature maps at the beginning of each level in the encoder part. The base number of filters was set to 16 and the number of filters were doubled at each level. Skip-connections were used like in the U-Net. The probability maps produced at the end of the decoder part of each sub-network had the same spatial size as the original image and were activated by a sigmoid function.

2.3 ResNet Block

He *et al.* [9] proposed the ResNet as a way to make training deep networks easier, and won the 1st place in the ImageNet Large Scale Visual Recognition Challenge (ILSVRC) 2015 classification task. It has been shown that ResNet-like networks are not only easier to optimize but also boost accuracy from considerably deeper networks [9,17]. Inspired by the winner of BraTS18 [17], we replaced the convolution blocks used in the traditional U-Net by ResNet blocks in two of our models (see Figure 2 and Table 1). An illustration of the ResNet-like block can be seen in Figure 3.

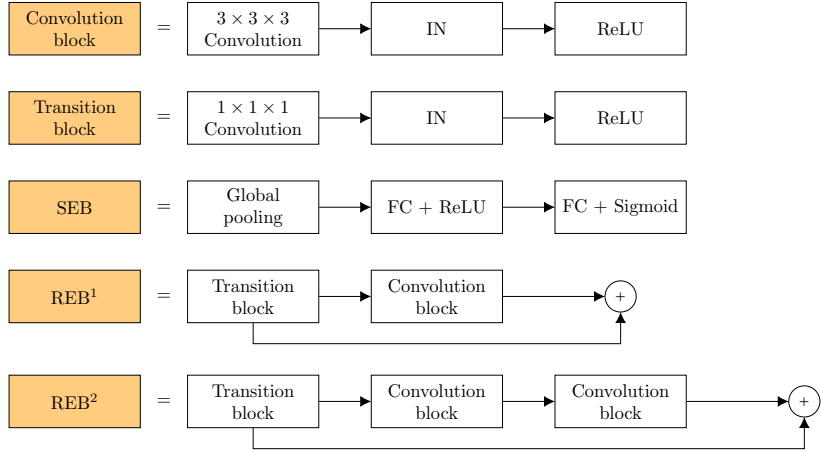


Fig. 3: The convolution blocks used in the different experiments (see Table 1). SEB, REB¹ and REB² denote Squeeze-and-Excitation block and two variations of ResNet blocks, respectively. Here, IN and FC stand for instance normalization and fully-connected layer, respectively; while rectified linear unit (ReLU) and Sigmoid are activation functions.

2.4 Squeeze-and-Excitation Block

We added a Squeeze-and-Excitation block (SEB) as developed by Hu *et al.* [12] after each convolution and concatenation block. The SEB is a computationally efficient means to incorporate channel-wise inter-dependencies, and has been widely used to improve network performances by significant margins [12]. SEB is also illustrated in Figure 3.

2.5 Preprocessing and Augmentation

We normalized all input images to have mean zero and unit variance. To increase the data set size, we employed simple on-the-fly data augmentation by randomly rotating the images within a range of -1 to 1 degrees and random mirror flips (on the x -axis) with a probability of 0.5. We also experimented with median denoising, but it did not demonstrate any additional improvements.

2.6 Post-processing

One of the most difficult tasks of BraTS19 is to detect small vessels in the tumor core and to label them as edema or as necrosis. To cope with the fact that LGG patients may have no enhancing tumor region, Isensee *et al.* [13] proposed to replace all enhancing tumor regions with less than 500 voxels by necrosis. We employed that approach in the present work as well. Additionally,

we kept decreasing the threshold segmentation from 0.5 to 0.3, 0.1, 0.05, and 0.01, respectively, if no core tumor region was found. This technique resolved several cases where the networks failed to distinguish between core and whole tumor.

2.7 Ensemble of Multiple Models

We employed five-fold cross-validation when training on the 335 cases (259 HGG + 76 LGG) of BraTS19, and did not use any additional in-house data. We trained 30 models in total and used 15 of them, that correspond to TuNet + SEB, TuNet + REB¹ + SEB and TuNet + REB² + SEB, to cast votes when predicting the final label maps. We used an average ensemble approach, such that

$$p_c = \frac{1}{M} \sum_{m=1}^M f_{mc}, \quad (1)$$

where $p_c \in \mathbb{R}^{|C|}$ and $f_{mc} \in \mathbb{R}^{|C|}$ denote the final probability of label c and the probability of label c generated by model m at an arbitrary voxel, respectively. Here, $C = \{1, 2, 3\}$ is the set of tumor labels, and thus $c \in C$.

The ensemble that we used was computed as the average of the prediction outputs of TuNet + SEB, TuNet + REB¹ + SEB and TuNet + REB² + SEB (see Table 1 and Table 2).

2.8 Task 3: Quantification of Uncertainty in Segmentation

In BraTS19, the organizers decided to include a new task that focuses on exploring uncertainty measures in the context of tumor segmentation on three glioma regions: whole, core, and enhancing. This task, called “Quantification of Uncertainty in Segmentation”, aimed at rewarding participating methods with resulting predictions that are: (a) confident when correct and (b) uncertain when incorrect. Participants were called on to generate uncertainty maps associated with the resulting labels at every voxel with values in [0, 100], where 0 represents the most certain prediction and 100 represents the most uncertain.

Our proposed approach, TuNet, benefits from this task since, fundamentally, it segments the brain tumor MRI images into three aforementioned tumor regions instead of partitioning into three labels. We define an uncertainty score, $u_{i,j,k}^r$, at voxel (i, j, k) as:

$$u_{i,j,k}^r = \begin{cases} 200(1 - p_{i,j,k}^r) & \text{if } p_{i,j,k}^r \geq 0.5 \\ 200p_{i,j,k}^r & \text{if } p_{i,j,k}^r < 0.5 \end{cases} \quad (2)$$

where thus $u_{i,j,k}^r \in [0, 100]^{|\mathcal{R}|}$ and $p_{i,j,k}^r \in [0, 1]^{|\mathcal{R}|}$ denote the uncertainty score map and probability map (the network’s likelihood outputs) corresponding to tumor region, $r \in \mathcal{R}$, as produced by the TuNet (see Figure 1), where \mathcal{R} is the set of tumor regions, *i.e.* whole, core, and enhancing region.

3 Experiments

We implemented our network in Keras¹ using TensorFlow² as the backend. This research was conducted using the resources of the High Performance Computing Center North (HPC2N)³ at Umeå University, Umeå, Sweden, and the experiments were run on NVIDIA Tesla V100 16 GB GPUs.

We report the results on the BraTS19 training set (335 cases) using cross-validation and on the validation set (125 cases) by uploading our predicted masks and corresponding uncertainty maps to the evaluation server. The evaluation metrics of Task 1—Segmentation included: DSC, sensitivity, specificity, and HD95; while the evaluation metrics of Task 3—Quantification of Uncertainty in Segmentation were Dice Area Under Curve (DAUC) and Ratio of Filtered True Positives (RFTPs).

3.1 Implementation Details and Training

For evaluation of the segmentation performance, we employed the DSC, defined as

$$D(X, Y) = \frac{2|X \cap Y|}{|X| + |Y|}, \quad (3)$$

where X and Y denote the output segmentation and its corresponding ground truth, respectively.

The HD95 is defined as the largest value in the set of closest distances between two structures, or

$$H(X, Y) = \max \left\{ \max_{x \in X} \min_{y \in Y} d(x, y), \max_{y \in Y} \min_{x \in X} d(y, x) \right\}, \quad (4)$$

where $d(x, y)$ denotes the Euclidian distance between two points $x \in X$ and $y \in Y$. It is common practice to report the 95th percentile instead of the maximum to compensate for outliers.

The loss function used for training contained three terms,

$$\mathcal{L}(u, v) = \mathcal{L}_{whole}(u, v) + \mathcal{L}_{core}(u, v) + \mathcal{L}_{enh}(u, v), \quad (5)$$

where \mathcal{L}_{whole} , \mathcal{L}_{core} , and \mathcal{L}_{enh} where the soft dice loss of whole, core, and enhancing tumor regions, respectively, and where the soft dice loss is defined as

$$\mathcal{L}_{dice}(u, v) = \frac{-2 \sum_i u_i v_i}{\sum_i u_i + \sum_i v_i + \epsilon}, \quad (6)$$

in which u is the softmax output of the network, v is a one-hot encoding of the ground truth segmentation map, and ϵ is a small constant added to avoid division by zero.

¹ <https://keras.io>

² <https://tensorflow.org>

³ <https://www.hpc2n.umu.se/>

Table 1: Mean DSC (higher is better) and HD95 (lower is better) and their standard deviations (SDs) (in parentheses) computed from the five-folds of cross-validation on the training set (335 cases) for the different models. Details of the variations of the convolution blocks used for each model is shown in Figure 3.

Model	DSC			HD95		
	whole	core	enh.	whole	core	enh.
TuNet	89.89 (2.07)	84.08 (4.02)	74.92 (7.24)	6.22 (2.66)	6.82 (2.93)	4.72 (2.21)
TuNet + SEB	91.38 (2.02)	85.93 (3.77)	78.11 (7.29)	4.50 (2.34)	6.70 (2.72)	4.24 (2.07)
TuNet + REB ¹	90.68 (1.98)	86.07 (3.84)	75.88 (7.36)	5.14 (2.07)	5.16 (1.99)	4.20 (1.99)
TuNet + REB ¹ + SEB	90.86 (2.12)	86.30 (3.72)	76.20 (7.32)	5.10 (2.29)	5.72 (2.62)	3.89 (1.61)
TuNet + REB ²	90.77 (2.18)	85.84 (3.96)	75.22 (7.30)	5.42 (2.50)	6.00 (2.38)	4.56 (2.09)
TuNet + REB ² + SEB	91.90 (2.00)	86.09 (3.81)	77.43 (7.28)	5.07 (2.38)	6.20 (2.45)	3.98 (1.87)
Ensemble	91.92 (2.18)	86.35 (3.81)	78.01 (7.30)	5.30 (2.19)	5.80 (2.69)	3.45 (1.93)
Ensemble + post-process	91.92 (2.18)	86.45 (3.79)	78.72 (7.10)	5.30 (2.19)	5.75 (2.65)	3.08 (1.90)

We used the Adam optimizer [14] with a learning rate of $1 \cdot 10^{-4}$ and momentum parameters of $\beta_1 = 0.9$ and $\beta_2 = 0.999$. We also used L_2 regularization with a penalty parameter of $1 \cdot 10^{-5}$, that was applied to the kernel weight matrices, for all convolutional layers to cope with overfitting. The activation function of the final layer was the sigmoid function.

All models were trained for 200 epochs, with a mini-batch size of four. To prevent over-fitting, we selected a patience period and dropped the learning rate by a factor of 0.2 if the validation loss did not improve over six epochs. Further, the training process was stopped if the validation loss did not improve after 15 epochs. The training time for a single model was around 35 hours on an NVIDIA Tesla V100 GPU.

4 Results and Discussion

The key strengths of the proposed method are: (1) it takes advantage of the hierarchical structure of the tumor sub-regions, since the whole tumor region must contain the core tumor, and the core tumor region must contain the enhancing tumor region, and (2) it consists of three connected sub-networks that mutually regularize each other, *i.e.* the E-Net functions as a regularizer for the C-net, C-Net plays that role for the W-Net, and the W-Net and the E-Net constrain each

Table 2: Results of Segmentation Task on BraTS19 validation data (125 cases). The results were obtained by computing the mean of predictions of five models trained over the folds. “UmU” denotes the name of our team and the ensemble of TuNet + SEB, TuNet + REB¹ + SEB and TuNet + REB² + SEB. The metrics were computed by the online evaluation platform. All the predictions were post-processed before submitting to the server. Bottom rows correspond to the top-ranking teams from the online system.

Model	DSC			HD95		
	whole	core	enh.	whole	core	enh.
TuNet + SEB	90.41	81.67	78.97	4.35	6.12	3.35
TuNet + REB ¹ + SEB	90.06	79.43	78.12	4.66	7.98	3.34
TuNet + REB ² + SEB	90.34	79.14	77.38	4.29	8.80	3.57
UmU	90.34	81.12	78.42	4.32	6.28	3.70
ANSIR	90.09	84.38	80.06	6.94	6.00	4.52
lfn_	90.91	85.48	80.24	4.35	5.32	3.88
SVIG1	91.16	85.79	81.33	4.10	5.92	4.21
NVDLMED	91.01	86.22	82.28	4.42	5.46	3.61

Table 3: Results of Quantification of Uncertainty Task on BraTS19 validation data (125 cases) including mean DAUC (higher is better) and RFTPs (lower is better). The results were obtained by computing the mean of predictions of five models trained over the folds. “UmU” denotes the name of our team and the ensemble of TuNet + SEB, TuNet + REB¹ + SEB and TuNet + REB² + SEB. The metrics were computed by the online evaluation platform. Bottom rows correspond to the top-ranking teams from the online system.

Model	DAUC			RFTPs		
	whole	core	enh.	whole	core	enh.
TuNet + SEB	87.52	79.90	75.97	4.50	12.97	6.59
TuNet + REB ¹ + SEB	86.13	80.01	75.13	5.80	16.50	8.02
TuNet + REB ² + SEB	87.40	79.32	75.90	5.50	15.30	8.53
UmU	87.47	79.86	75.89	5.83	13.72	8.46
ANSIR	89.42	88.72	87.67	1.23	6.16	4.63
NVDLMED	89.95	88.03	84.67	1.68	2.43	2.86
TEAM_ALPACA	90.93	88.08	87.90	1.54	3.82	2.59

other through the C-Net. An adapted version of the TuNet was also used by the authors in the Kidney Tumor Segmentation Challenge 2019 (KiTS19) [10].

Table 1 shows the mean DSC and HD95 scores and SDs computed from the five-folds of cross-validation on the training set. As can be seen in Table 1, with

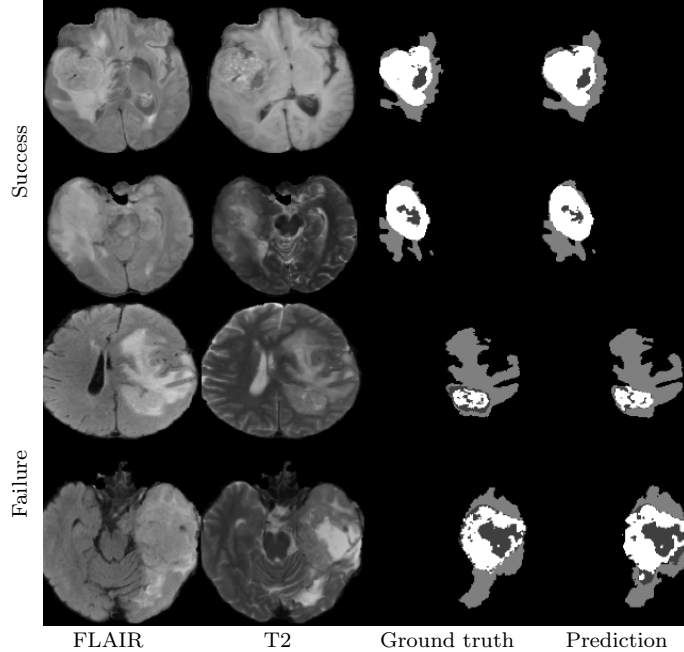


Fig. 4: A comparison of the ground truth masks and the results. The two examples show the input T1c (left), the ground truth masks (middle) and the results of the proposed method (right).

DSC of 89.89/84.08/74.92 (whole/core/enh.) using cross-validation on the training set and 89.70/76.96/77.90 (whole/core/enh.) on the validation set, our *baseline* (TuNet) produced acceptable results. Adding SEB to TuNet (TuNet + SEB) improved the DSC on all tumor regions; however, only core and core+enhancing DSC scores were boosted when adding SEB to two variations, that used ResNet-like blocks, *i.e.* TuNet + REB¹ + SEB and TuNet + REB² + SEB.

We gained a few DSC points when the average ensemble technique (Ensemble), *i.e.* DSC reached 91.92/86.45/78.72 (whole/core/enh.). The post-processing step only improved slightly the Ensemble model on the core region, but boosted the DSC of the enhancing region by a large margin, from 78.01 to 78.72, making it (Ensemble + post-processing) the best-performing model of all proposed models on the training set.

Table 2 shows the mean DSC and HD95 scores on the validation set by uploading our predicted masks to the evaluation server⁴ (team name *UmU*). What is interesting in this table is: (1) DSC of core region on the validation set was lower compared to the cross-validation score on the training set, and (2) TuNet + SEB, perhaps surprisingly, performed slightly better than the ensemble

⁴ <https://www.cbica.upenn.edu/BraTS19/lboardValidation.html>

model of TuNet + SEB, TuNet + REB¹ + SEB and TuNet + REB² + SEB. A possible explanation for these results might be that: it might be due to the relatively small size of the validation set (125 cases compared to 335 training cases).

Table 3 provides the mean DAUC and RTPs scores on the validation set obtained after uploading our predicted masks and corresponding uncertainty maps to the evaluation server⁵. Similar to Table 2, it can be seen in Table 3 that TuNet + SEB is the best-performing model of our models. Though our best-performing model performs worse than the top-ranking teams on the validation set, it was one of the top-performing models on the test set (we were contacted by the organizers, details will be updated after the leaderboard is released). This might due to a fact that our proposed ensemble method generalizes the problem well.

Figure 4 illustrates four qualitative examples generated from the Ensemble + post-process model on the training set. As can be seen in the first and second rows, our model detected all three regions well. However, it struggled to correctly differentiate between the necrotic and non-enhancing tumor core and the enhancing tumor (third and last rows). This is most likely due to difficulties in labeling the homogeneous areas.

Figure 5 illustrates the uncertainty score maps generated from corresponding probability maps, that are produced by our TuNet, for three tumor regions (whole, core, and enhancing). As can be seen in Figure 5, the uncertainty scores tends to be: (i) more obvious at the borderline or overlapping areas between tumor regions, and (ii) less apparent on the background or non-tumor regions.

5 Conclusion

In conclusion, we developed a cascaded architecture by connecting three U-Net-like networks to segment glioma sub-regions from multimodal brain MRI images. We separated the complex brain tumor segmentation into three simpler binary tasks to segment the whole tumor, tumor core, and enhancing tumor core, respectively. Our network used an encoder-decoder structure with ResNet-like blocks and Squeeze-and-Excitation blocks after each convolution and concatenation block. Dice scores on the training set and validation set were respectively 91.92/86.45/78.72 and 90.34/81.12/78.42 for the whole tumor, tumor core, and enhancing tumor core.

References

1. Asklund, T., Björ, O., Malmström, A., Blomquist, E., Henriksson, R.: Överlevnanden vid maligna gliom har ökat senaste tio åren. analys av kvalitetsregisterdata. *Läkartidningen* **109**(17-18), 875–878 (2012)

⁵ <https://www.cbica.upenn.edu/BraTS19//lboardValidationUncertainty.html>

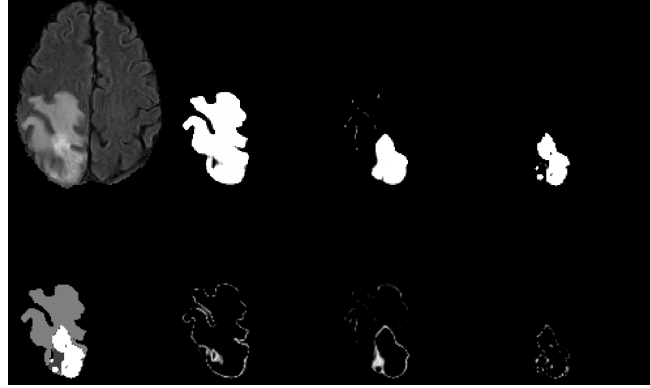


Fig. 5: The uncertainty score maps generated from probability maps corresponding to whole, core, and enhancing tumor regions. Top row (from left to right): input, probability map of the whole, core and enhancing tumor regions, respectively. Bottom row (from left to right): multi-class label map (output), uncertainty map of the whole, core and enhancing tumor regions, respectively.

2. Bakas, S., Akbari, H., Sotiras, A., Bilello, M., Rozycki, M., Kirby, J., Freymann, J., Farahani, K., Davatzikos, C.: Segmentation labels and radiomic features for the pre-operative scans of the tcga-gbm collection. the cancer imaging archive (2017) (2017)
3. Bakas, S., Akbari, H., Sotiras, A., Bilello, M., Rozycki, M., Kirby, J., Freymann, J., Farahani, K., Davatzikos, C.: Segmentation labels and radiomic features for the pre-operative scans of the tcga-lgg collection. The Cancer Imaging Archive **286** (2017)
4. Bakas, S., Akbari, H., Sotiras, A., Bilello, M., Rozycki, M., Kirby, J.S., Freymann, J.B., Farahani, K., Davatzikos, C.: Advancing the cancer genome atlas glioma MRI collections with expert segmentation labels and radiomic features. Scientific data **4**, 170117 (2017)
5. Bakas, S., Reyes, M., Jakab, A., Bauer, S., Rempfler, M., Crimi, A., Shinohara, R.T., Berger, C., Ha, S.M., Rozycki, M., et al.: Identifying the best machine learning algorithms for brain tumor segmentation, progression assessment, and overall survival prediction in the BRATS challenge. arXiv preprint arXiv:1811.02629 (2018)
6. Boser, B.E., Guyon, I.M., Vapnik, V.N.: A training algorithm for optimal margin classifiers. In: Proceedings of the fifth annual workshop on Computational learning theory. pp. 144–152. ACM (1992)
7. Chen, L.C., Zhu, Y., Papandreou, G., Schroff, F., Adam, H.: Encoder-decoder with atrous separable convolution for semantic image segmentation. In: Proceedings of the European conference on computer vision (ECCV). pp. 801–818 (2018)
8. Gholami, A., Mang, A., Biros, G.: An inverse problem formulation for parameter estimation of a reaction–diffusion model of low grade gliomas. Journal of mathematical biology **72**(1-2), 409–433 (2016)

9. He, K., Zhang, X., Ren, S., Sun, J.: Deep residual learning for image recognition. In: Proceedings of the IEEE conference on computer vision and pattern recognition. pp. 770–778 (2016)
10. Heller, N., Sathianathan, N., Kalapara, A., Walczak, E., Moore, K., Kaluzniak, H., Rosenberg, J., Blake, P., Rengel, Z., Oestreich, M., Dean, J., Tradewell, M., Shah, A., Tejpaul, R., Edgerton, Z., Peterson, M., Raza, S., Regmi, S., Papanikolopoulos, N., Weight, C.: The KiTS19 challenge data: 300 kidney tumor cases with clinical context, CT semantic segmentations, and surgical outcomes (2019)
11. Holland, E.C.: Progenitor cells and glioma formation. *Current opinion in neurology* **14**(6), 683–688 (2001)
12. Hu, J., Shen, L., Sun, G.: Squeeze-and-excitation networks. In: Proceedings of the IEEE conference on computer vision and pattern recognition. pp. 7132–7141 (2018)
13. Isensee, F., Kickingereder, P., Wick, W., Bendszus, M., Maier-Hein, K.H.: No new-net. In: International MICCAI Brainlesion Workshop. pp. 234–244. Springer (2018)
14. Kingma, D.P., Ba, J.: Adam: A method for stochastic optimization. *arXiv preprint arXiv:1412.6980* (2014)
15. Kittrungrotsakul, T., Iwamoto, Y., Han, X.H., Takemoto, S., Yokota, H., Ipponjima, S., Nemoto, T., Wei, X., Chen, Y.W.: A cascade of CNN and LSTM network with 3D anchors for mitotic cell detection in 4D microscopic image. In: ICASSP 2019-2019 IEEE International Conference on Acoustics, Speech and Signal Processing (ICASSP). pp. 1239–1243. IEEE (2019)
16. Menze, B.H., Jakab, A., Bauer, S., Kalpathy-Cramer, J., Farahani, K., Kirby, J., Burren, Y., Porz, N., Slotboom, J., Wiest, R., et al.: The multimodal brain tumor image segmentation benchmark (BRATS). *IEEE transactions on medical imaging* **34**(10), 1993–2024 (2014)
17. Myronenko, A.: 3D MRI brain tumor segmentation using autoencoder regularization (2018), <http://arxiv.org/abs/1810.11654>
18. Ronneberger, O., Fischer, P., Brox, T.: U-Net: Convolutional networks for biomedical image segmentation. In: International Conference on Medical image computing and computer-assisted intervention. pp. 234–241. Springer (2015)
19. Wang, G., Li, W., Ourselin, S., Vercauteren, T.: Automatic brain tumor segmentation using cascaded anisotropic convolutional neural networks. *Lecture Notes in Computer Science* p. 178190 (2018)